https://doi.org/10.5194/egusphere-2026-993
Preprint. Discussion started: 17 March 2026

Ocean and marine heatwaves responses to multiple net-zero worlds

Isaline Bossert[1], Roland Séférian[1], Yeray Santana-Falcón[2] and Thibault Guinaldo[1]

[1] Météo-France, CNRS, Univ. Toulouse, CNRM, Toulouse, France
[2] Instituto de Oceanografía y Cambio Global, Universidad de Las Palmas de Gran Canaria, Telde, Spain

Correspondence to: Isaline Bossert (isaline.bossert@meteo.fr)

Abstract. Climate change profoundly modifies the global ocean potentially threatening marine ecosystems. Under the Paris Agreement, the international community aims to limit global warming by achieving net-zero CO_2 emissions, through the balance between CO_2 emissions and removals. Yet, the response of the ocean to net-zero, and associated impacts, remains poorly understood. Prevailing Global Warming Level (GWL) approaches applied to analyse the impacts of climate change on the ocean overlook committed changes arisen after emissions cessation. Using the CNRM-ESM2-2 Earth system model, we perform 300-year net-zero simulations spanning +1.1 °C to +5 °C above pre-industrial levels, to investigate the ocean responses to CO_2 emissions cessation, and how they depend on the warming level at which net-zero emissions is reached. Focusing on sea surface temperature (SST) and marine heatwaves (MHW) – key threats for marine ecosystems – we find substantial departures from transient responses throughout the 300-years of stabilization. At the Paris Agreement targets of +1.5 °C and +2.0 °C above pre-industrial levels, 26 % and 32 % of the global ocean, respectively, exhibit simultaneous increases in SST mean and variance as compared to transient warming simulations. These changes cover particularly the high latitudes and Southern ocean. MHW reorganize rapidly after emissions cease, with a poleward shift in frequency, declines in the tropics, and overall sustained intensity. Altogether, these non-transient responses indicate that standard GWL approaches underestimate MHW reorganization by decades to centuries. Net-zero simulations are therefore critical for robust projections of marine ecosystem risk at stabilized global warming levels.

1 Introduction

The Paris Agreement aims to halt "the increase in the global average temperature to well below 2ºC above pre-industrial levels", pursuing efforts to limit warming to 1.5ºC (UNFCCC, 2015). It assumes most climate impacts will slow or stabilize once incremental warming ceases, as observations link multiple impacts to rising warming (C. D. Jones et al., 2019; MacDougall et al., 2020; Palazzo Corner et al., 2023). This has driven widespread use of the global warming level (GWL) approach: extracting periods of a few decades centered on target GWL from continuously warming future projections (Frölicher et al., 2018; King et al., 2017). This framework underpinned key assessments, including the Special Report on global warming of 1.5 °C (IPCC SR1.5, Masson-Delmotte et al., 2018). Yet stabilizing global climate at warming targets requires reaching net-zero CO_2 emissions (Matthews & Caldeira, 2008), which reveal limitations in transient projections, where global mean surface air temperature (GMSAT) keeps rising through analysis windows. Such frameworks thus miss

https://doi.org/10.5194/egusphere-2026-993
Preprint. Discussion started: 17 March 2026

the equilibrium dynamics of the Earth system and long-term spatio-temporal evolution under stable conditions, challenging the Paris Agreement (King et al., 2020, 2021).

Several protocols have emerged to simulate stabilized GWL (SWL, C. Jones et al., 2025; C. D. Jones et al., 2019; Sanderson et al., 2025; Terhaar et al., 2022). Although idealized and feasibility-debated, these pathways represent optimistic scenarios for constraining climate below temperature thresholds. However, stabilizing GMSAT does not equate to the steady-states of other Earth system components (Lacroix et al., 2024; Palazzo Corner et al., 2023; Silvy et al., 2024; Terhaar et al., 2023). Indeed, Silvy et al., (2024) and Lacroix et al., (2024) show a decline of the Atlantic meridional overturning circulation (AMOC) and sea-ice concentration when GMSAT is halted to +2 °C, followed by a recovery several decades later due to Earth system feedback. On the other hand, Lacroix et al., (2024) and Terhaar et al. (2023) showed that some fields, such as sea level rise or ocean acidification, continue evolving independently from GMSAT stabilization.

The ocean plays a key role by slowing down the rate of atmospheric CO_2 accumulation (i.e. carbon pump, Canadell et al., 2021) and absorbs approximately 90 % of excess heat accumulation resulting from the positive Earth's energy imbalance related to anthropogenic emission of greenhouse gases (von Schuckmann et al., 2023), making it the Earth system's primary heat reservoir. Nonetheless, the ocean exhibits a strong thermal inertia. It has been shown that it keeps taking up heat over decadal to centennial scales even without added radiative forcing (Gillett et al., 2011; MacDougall et al., 2020). Net-zero simulations thus reveal ocean responses and impacts distinct from those expected in transient GWL analyses focused on short windows, potentially underestimating the full adjustment at a given GWL.

Within this context, concern is growing regarding socio-economic and ecosystemic impacts of global warming (Doney et al., 2012; Smith et al., 2021). Multiple lines of evidence report the ecological consequences of ocean warming for organisms (Pörtner & Farrell, 2008), including observed poleward shifts of major phytoplankton communities (Hutchins & Tagliabue, 2014). Furthermore, enhanced thermal variability and more frequent extreme temperature events, referred to as marine heatwaves (MHW, Hobday et al. 2016, Oliver et al. 2021), may exert physiological stress or even mortality of organisms that can overweight the sole response to shift in the mean temperature (Smith et al., 2023; Vasseur et al., 2014; Wernberg et al., 2025). These events – attributable to anthropogenic climate warming – are projected to intensify in frequency, duration, and intensity under transient anthropogenic emissions (Capotondi et al., 2024; Frölicher et al., 2018; Laufkötter et al., 2020). Overall, changes in the shape of temperature distributions as well as changes in vertical temperature ranges are shown to impact marine ecosystems (Guinaldo & Neukermans, 2026; Santana-Falcón & Séférian, 2022).

Despite this urgency, ocean responses to climate stabilization – particularly shifts in temperature distributions and extreme events like MHW – remain poorly investigated. Here, we fill this gap by using the TipMIP protocol (C. Jones et al., 2025), which consists in shutting down CO_2 emissions once target temperatures are reached after a continuous global warming ramp-up stage. The stabilization, then, rests on reaching an equilibrium between (i) a cooling effect due to a decrease in radiative forcing and (ii) a warming effect linked to heat transfer at the sea surface to the atmosphere (MacDougall et al., 2020; Palazzo Corner et al., 2023).

https://doi.org/10.5194/egusphere-2026-993
Preprint. Discussion started: 17 March 2026

In the present study, we specifically aim to broaden our understanding on (i) how the ocean will respond to CO_2 emission cessation, and (ii) how this response is modulated by the level of warming at which net-zero emissions are reached. We extend the TipMIP protocol with nine net-zero CO_2 emission simulations using the CNRM-ESM-2-2 model. They span SWLs from +1.1 °C to +5.0 °C relative to pre-industrial levels (evenly sampled each 0.5 °C). We focus on sea surface temperature (SST) distributions and MHW which are key indicators of risks for marine ecosystems. Simulations, methods and definitions are described in Sect. 2.2. We characterize global stabilization results in Sect. 3.1. Then, Sect. 3.2 dives into the analysis of SST distributions. Finally, we investigate the evolution of marine heatwaves frequency and intensity, through time and in-between the transient and stabilized storylines in Sect. 3.3.

2 Methods

2.1 CNRM-ESM2-2

This study analyzes model outputs of CNRM-ESM2-2 (Bossert et al., 2025), the improved version of the Earth System model of second generation developed by CNRM-CERFACS. Compared to its previous version (CNRM-ESM2-1, Séférian et al., 2019), CNRM-ESM2-2 offers an improved representation of the global carbon cycle, of several Earth system interactions (aerosols-light, biophysics, etc.) as well as an improved treatment of the anthropogenic disturbance on land.

The atmosphere component of CNRM-ESM2-2 is based on version 6.3 of the global spectral model ARPEGE-Climat (ARPEGE-Climat_v6.3, Roehrig et al., 2020). ARPEGE-Climat resolves atmospheric dynamics and thermodynamics on a T127 triangular grid truncation that offers a spatial resolution of about 150 km in both longitude and latitude. CNRM-ESM2-2 employs a "high-top" configuration with 91 vertical levels that extend from the surface to 0.01 hPa in the mesosphere; 15 hybrid σ-pressure levels are available below 1500 m.

The ocean component of CNRM-ESM2-2 is the Nucleus for European Models of the Ocean (NEMO) version 3.6 (Madec et al., 2017) which is coupled to both the Global Experimental Leads and ice for ATmosphere and Ocean (GELATO) sea-ice model (Salas Mélia, 2002) version 6 and the marine biogeochemical model Pelagic Interaction Scheme for Carbon and Ecosystem Studies version 2-gas (PISCESv2-gas, Aumont et al., 2015; Berthet et al., 2023). NEMOv3.6 operates on the eORCA1L75 grid (Mathiot et al., 2017) which offers a nominal resolution of 1° to which a latitudinal grid refinement of 1/3° is added in the tropics. This grid describes 75 ocean vertical layers using a vertical z*-coordinate with partial step bathymetry formulation (Bernard et al., 2006).

https://doi.org/10.5194/egusphere-2026-993
Preprint. Discussion started: 17 March 2026

2.2 Simulation protocol

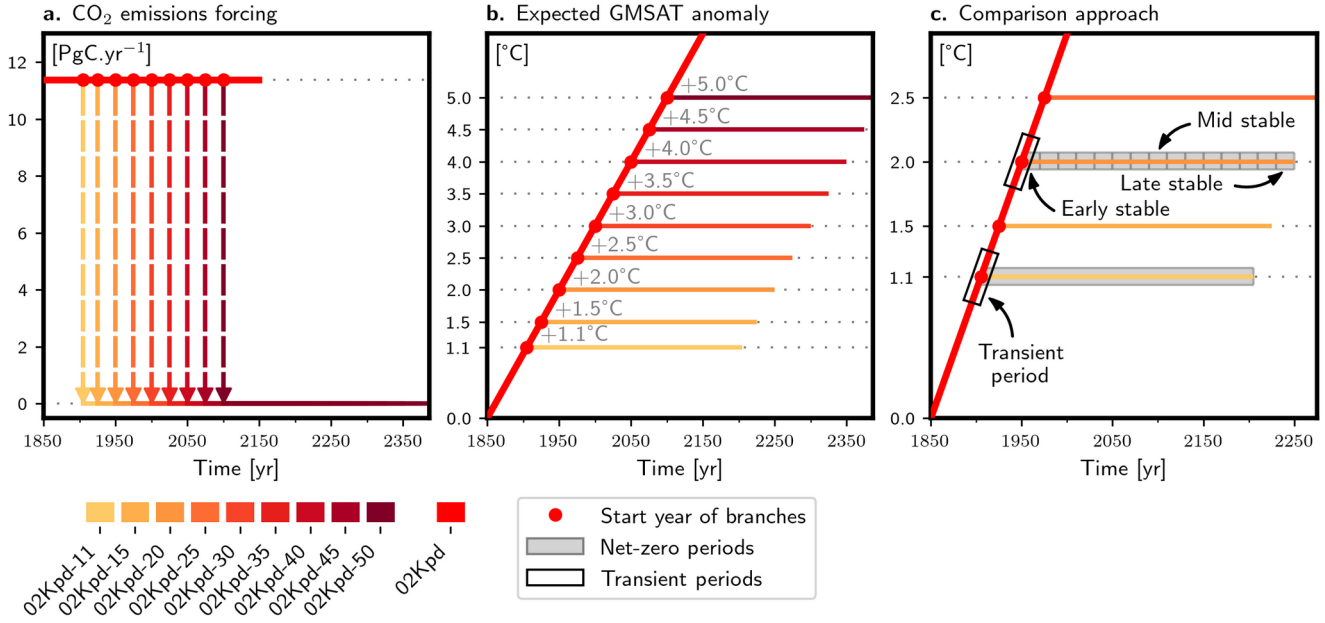

Figure 1. Stabilization protocol schemes. Schemes illustrating the CO_2-emissions forcing parameterization and the expected global mean surface air temperature (GMSAT). Panel (a) illustrates the forcings for the ramp-up run (red thick line) are set to 11,378 PgC yr^{-1}. These emissions are then successively shut down for each net-zero branch (arrows going from yellow to dark red as the global warming target is increasing) which keep running after emission cessation. Panel (b) shows the expected GMSAT during the ramp-up and net-zero stages of the experiment. A zoom in the later panel is plotted in (c) and displays the two comparison approaches used in this study. Black outlined boxes show the 21-year periods taken from the transient ramp-up at each global warming levels and gray shaded boxes show the 21-year or 300-year of data extracted in the net-zero runs. (a-c) Colors grading from yellow to dark red stand for the different net-zero runs. The red curve is the ramp-up simulation with corresponding round markers showing the years where net-zero runs start.

Using the CNRM-ESM2-2 model, we produced nine multicentennial-long simulations in which CO_2 emissions are brought abruptly to zero and where, in consequence, GMSAT is expected to stabilize at various GWL (see Fig. 1). This section describes the experimental protocol employed to generate such simulations.

CNRM-ESM2-2 simulations were performed in emission-driven mode, a framework where the model computes the evolution of atmospheric CO_2 thanks to the simulated global carbon cycle and to prescribed monthly-updated net anthropogenic CO_2 emissions. This mode is chosen because only emission-driven models can capture the balance between the ocean heat/carbon storage and atmospheric CO_2 radiative forcing, which is essential to realistically model the response to net-zero emissions (MacDougall et al., 2020).

We first ran a 500-year emission-driven preindustrial control simulation (esm-piControl hereafter) following CMIP6 protocol (Eyring et al., 2016), from which we can infer the GWL (taken as the warming from the preindustrial mean climate). From the esm-piControl simulation, we branched an idealized simulation aiming to model a GMSAT increase of

https://doi.org/10.5194/egusphere-2026-993
Preprint. Discussion started: 17 March 2026

+0.2 °C per decade (02Kpd experiment). This level of warming replicates the current observed global warming rate (Matthews & Wynes, 2022). Achieving the 02Kpd ramp-up simulation requires linking the target GMSAT increase (ΔT) to the monthly cumulative CO_2-emissions prescribed to force the CNRM-ESM2-2 (ΔE).

ΔE is derived from the transient climate response to cumulative CO_2 emission (TCRE) of CNRM-ESM2-2, which was computed following Arora et al., (2020). The ratio between ΔT and the TCRE results in the amount of yearly CO_2 emissions, i.e., ΔE, to be prescribed in our emission-driven model in order to perform the 02Kpd simulation. Here our TCRE equals 1.758 °C Eg C^{-1}, and ΔT is +0.02 °C yr^{-1}. Thus, we distribute a global forcing ΔE of 11.378 Pg C yr^{-1} propagated uniformly on each model grid cell and evenly distributed monthly.

Figure 1a-b illustrates the protocol to generate the nearly stabilized GMSAT simulations. We monitored the 02Kpd simulation to check when the 31-years rolling-mean GMSAT anomaly reaches the first GWL target, which is +1.1 °C relative to pre-industrial mean (taken as the mean of the esm-piControl simulation) in order to represent current observed global warming levels. The 31-years rolling-mean, recommended in Jones et al., (2025), ensures that the GWL is reached at a climatological scale and is not just the result of a warmer year due to natural variability. When reaching this target, CO_2 emissions are set to zero (top-to-bottom arrow in Fig. 1a), and a net-zero branch is started on January 1st of that year. The same procedure is done for the subsequent GWL targets (i.e. spanning from +1.5 °C to +5.0 °C every 0.5 °C increments). We end up with nine 300-year net-zero branches called 02Kpd-XX, where XX is the respective GWL target (see the experiment identifications in Table 1) .

2.3 Analysis framework and diagnostics

2.3.1 Comparison approach

Table 1. Summary of the transient and net-zero CO_2 emissions experiments associated with their global warming levels (GWL) targets. The beginning and end year of each run is given. Transient baselines for each GWL are the 21-year periods baselines extracted from the 02Kpd experiment to be compared with the 300-years of stabilization or the three 21-year periods called early-stable, mid-stable and late-stable.

GWL	Experiment ID	Span in time (SWL_{300})	Transient baseline (TWL)	Early stable (SWL_{21})	Mid stable (SWL_{21})	Late stable (SWL_{21})
Transient framework						
-	02Kpd	1850-2149	-	-	-	-
Net-zero framework						
+1.1 °C	02Kpd-11	1902-2201	1892-1912	1902-1922	2042-2062	2181-2201
+1.5 °C	02Kpd-15	1923-2222	1913-1933	1923-1943	2063-2083	2202-2222

https://doi.org/10.5194/egusphere-2026-993
Preprint. Discussion started: 17 March 2026

+2.0 °C	02Kpd-20	1949-2248	1939-1959	1949-1969	2089-2019	2228-2248
+2.5 °C	02Kpd-25	1972-2271	1962-1982	1972-1992	2112-2132	2251-2271
+3.0 °C	02Kpd-30	1997-2296	1987-2007	1997-2017	2137-2157	2276-2296
+3.5 °C	02Kpd-35	2022-2321	2012-2032	2022-2042	2162-2182	2301-2321
+4.0 °C	02Kpd-40	2044-2343	2034-2054	2044-2064	2184-2204	2323-2343
+4.5 °C	02Kpd-45	2066-2365	2056-2076	2066-2086	2206-2226	2345-2365
+5.0 °C	02Kpd-50	2087-2386	2077-2097	2087-2107	2227-2247	2366-2386

One aim of this study is to analyze (i) how ocean temperature distributions and extremes will respond to CO_2 emission cessation and (ii) how this response is modulated by the level of warming at which net-zero emissions is reached. Therefore, we need to track changes between transient and net-zero CO_2 emissions simulations at the same GWL.

In the following, we will distinguish stabilized warming levels (SWLs) and transient global warming levels (TWLs). SWL generally refers to net-zero CO_2 emission simulations at a given GWL whereas TWL refers to the 21-year periods centered around the year when a given GWL is reached in the ramp-up simulation (see Sect. 2.3.3). This time window is consistent with IPCC AR6 practices (Eyring et al., 2021).

In this regard, two comparison approaches are employed here. In the first approach, we consider each 300-years net-zero experiment as a whole (gray shaded box shown for 02Kpd-11 in Fig. 1c). They will be referred to as SWL_{300}. In the second approach, we define SWL_{21} as individual 21-year time periods extracted from the 02Kpd-XX experiments (gray shaded boxes shown for 02Kpd-20 in Fig. 1c). It provides insights into the possible temporal evolution appearing throughout net-zero. We focus mostly on the first, mid and last 21-year of net-zero, respectively referred to as early-, mid- and late-stable. We compare the SWL_{300} and SWL_{21} states with their respective TWL states (black outlined boxes in Fig. 1c). The complete comparison method is schematized in Fig. 1c for 02Kpd-11 (first approach) and 02KPd-20 (second approach). An inventory of the time periods for transient, early-, mid- and late-stable is presented in Table 1.

2.3.2 Global averages and metrics definitions

Global averages and metrics are calculated to inform on the overall behaviour of the Earth system after CO_2 emissions cessation for all runs. Surface air temperature, atmospheric CO_2 concentration, and sea surface temperature are calculated as area-weighted global means, using the surface area of each grid cell as weights. These global variables are referred to as GMSAT, GMCO2, and GMSST, respectively. Anomalies relative to the pre-industrial mean state are named ΔGMSAT,

https://doi.org/10.5194/egusphere-2026-993
Preprint. Discussion started: 17 March 2026

ΔGMCO2, and ΔGMSST. We also evaluate in depth ocean temperature with a subsurface layer (10-70m) and a deeper layer (100-500m). Their global averages are evaluated by applying a grid cell volume weighted mean.

The temporal evolution of radiative forcings (ΔRF) was derived from GMCO2 using the relationship from Myhre et al., (1998) expressed in Eq. (1) with t_0 the year where the net-zero run starts.

$$\Delta RF(t) = 5.35 \ln\left(\frac{GMCO2(t)}{GMCO2(t_0)}\right), \quad (1)$$

The ocean heat uptake (ΔOHU) was globally integrated and calculated as a departure from its initial value (t_0). Conventions for both ΔRF and ΔOHU were taken as positive fluxes when reaching the atmosphere. To address the imbalance between ΔRF and ΔOHU after net-zero, we compute the difference between the two variables. The AMOC index is defined as the in-depth maximum of the meridional stream function at 26 °N.

Finally, we assess Zero Emission Commitment (ZEC) metrics for each net-zero run and at various time horizons after emissions cessassion noted ZEC_t. As in MacDougall et al., (2020), they are defined relative to the year where emissions cease (t_0) and averaged over a 21-year window centered around year t., as expressed in Eq. (2). In addition, we evaluate an overall ZEC defined over the whole 300-years of net-zero.

$$ZEC_t = \frac{1}{21}\sum_{k=t-10}^{t+10}\left(GMSAT(k) - GMSAT(t_0)\right), \quad (2)$$

2.3.3 Distribution of SST anomalies

We compute the daily SST anomalies in the 02Kpd simulation and in the various 02Kpd-XX simulations as departure from a daily climatological cycle smoothed with a 31-days running average. We choose the 21-year transient time periods TWL as baselines for our climatological cycles. We then look at the first two statistics of the SST anomaly distributions for each GWL and each framework. Statistics over the SWL_{300} time periods are made on daily 300-year samples ($n \approx 109800$) while those calculated over the SWL_{21} and TWL periods are made on daily 21-year samples ($n \approx 7686$).

Statistic's name are shortened as follows: mean (μ) and standard-deviation (σ). An increase of each of these statistics would imply a greater risk of facing extreme events for species sensitive to higher environmental temperature. We compare μ and σ in the net-zero and in the transient framework using the approaches described in Sect. 2.3.1. Skewness is not shown here, nonetheless focus has been put on MHW which also inform on the tail of the distribution.

We used various parametrical and non-parametrical statistical tests to assess if samples in the net-zero simulations are significantly different from the transient samples in terms of mean, variance and followed statistical law. First, the parametrical Welch t-test (Welch, 1947) was applied to test the null hypothesis that two samples have the same mean. It enables testing samples of different length and it has the advantage of being reliable when samples have unequal variance.

https://doi.org/10.5194/egusphere-2026-993
Preprint. Discussion started: 17 March 2026

Then, to test for the statistical significance of different variance between the transient and the net-zero samples we used the parametrical Levene t-test (Levene, 1960). Finally, we applied a Kolmogorov-Smirnov non-parametric test (Massey Jr., 1951) to check if the shape of the distribution in the net-zero simulations are deemed significantly different from the distribution of their respective transient baseline (TWL). For all these tests, we reject the null hypothesis if the p-value is below the 5 % significance level.

Furthermore, we applied a False Discovery Rate (FDR, Benjamini & Hochberg, 1995) on our p-values to avoid false significance in isolated grid cells and overestimation of significance due to spatial autocorrelation.

2.3.4 Marine heatwaves definitions

Marine heatwaves are discrete events where the SST is anomalously high, exceeding a given threshold for a given period of time. Many definitions exist and they mainly lie on a choice of baselines, duration of exceedance as well as thresholds which depend on the intended application (Amaya et al., 2023; Hobday et al., 2016; Oliver et al., 2021; Smith et al., 2023).

MHW are here defined using a seasonally varying daily climatological threshold corresponding to the 90th percentile of the local daily SST distribution. Using this definition, temperature extremes lie in the warm tails of the SST distributions. Therefore, they supplement the information given by the SST anomalies distributions described in Sect. 2.3.3. The daily percentile seasonal cycle is smoothed using a 31-days running average to get rid of noise in the low-sampled seasonal cycle as was done in Le Grix et al., (2021). We do not spatially gather coherent gridcell facing a MHW. Furthermore, no duration threshold was used in this study, since relevance of a duration threshold is highly arbitrary as may vary among studied processes and impacts. However, this choice has some limitations since the ecological implications of short-lived and prolonged MHW can differ markedly and are not distinguished in this study.

Here, to compare transient and net-zero schemes we chose as baselines the TWL periods defined in Table 1 (see also black outlined boxes in Fig. 1c). Hence, each net-zero run has its own baseline defined in the transient space (TWL). The choice of a fixed baseline is motivated by the fact that we want to compare two different frameworks and especially changes between transient and stabilized worlds. From an ecological perspective, however, the use of a fixed transient baseline may not fully capture the relevance of MHW in a steady ocean warming where organisms may adapt to shifting thermal regimes or shift their position to more favorable conditions if possible (Amaya et al. 2023).

Extreme events are detected in the transient (21-year) and the net-zero time series (300 years). Two metrics were investigated: frequency and intensity. MHW intensity is defined as the temperature exceedance above the 90th percentile threshold. MHW frequency is defined as the number of days facing an extreme over the total number of days in the considered time series (21 years for TWL and SWL_{21} and 300 years for SWL_{300}).

https://doi.org/10.5194/egusphere-2026-993
Preprint. Discussion started: 17 March 2026

3 Results and discussion

3.1 Global climate state after net-zero emission

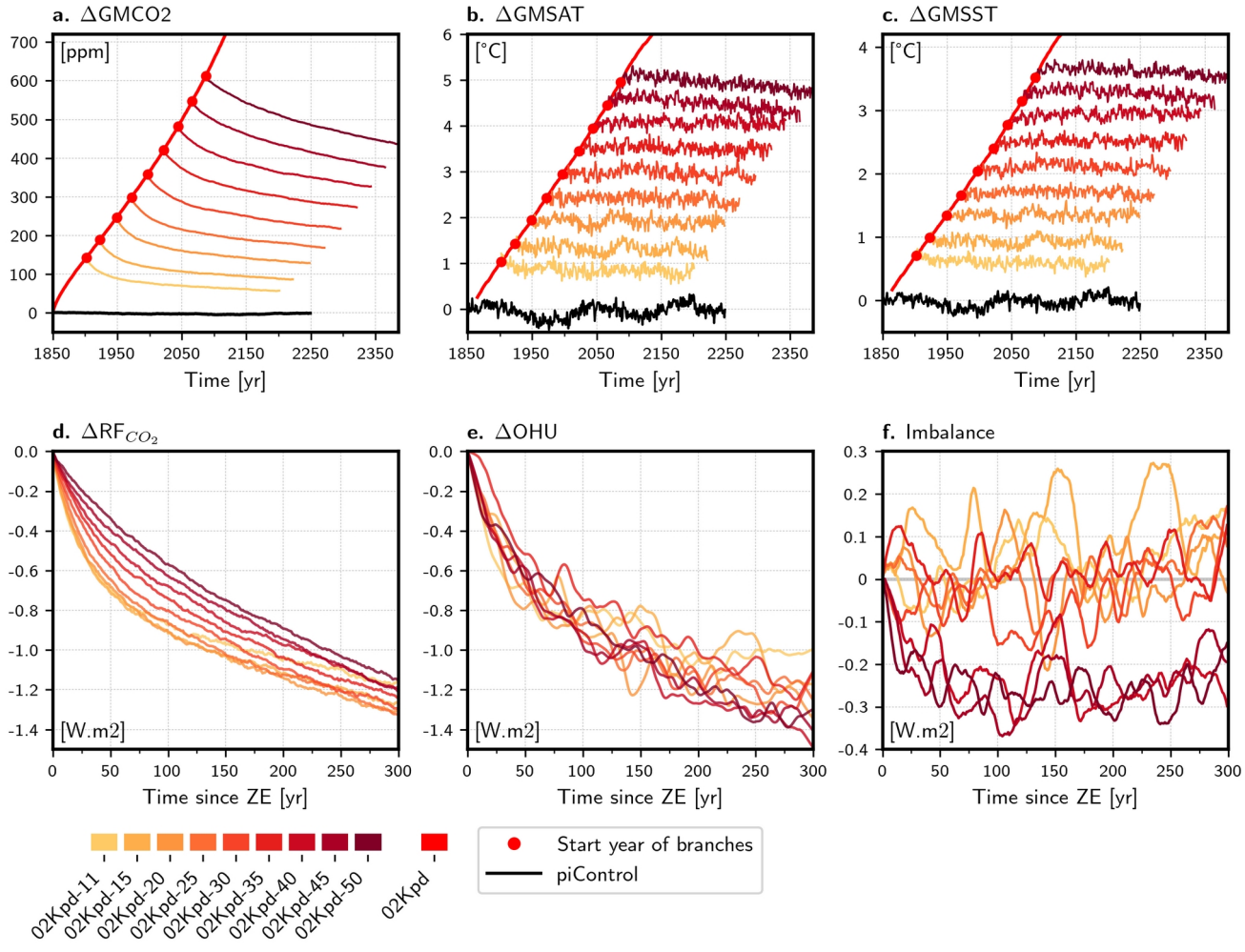

Figure 2. Climate climate state during ramp-up and net-zero. Outputs of the ramp-up and net-zero runs for (a) atmospheric CO_2 concentration (GMCO2), (b) global mean surface air temperature (GMSAT), (c) global mean sea surface temperature (GMSST), (d) anomalies in radiative forcing (ΔRF_{CO2}), (e) anomalies in ocean heat uptake (ΔOHU) and (f) the energy imbalance between ΔOHU and ΔRF_{CO2}. Colors grading from yellow to dark red stand for the different net-zero runs. The pre-industrial control is shown in black. The red curve is the +0.2 °C per decade ramp-up simulation with corresponding round markers showing the years where net-zero runs start. ΔOHU and ramp-ups are smoothed with LOWESS regressions and 31-year running-mean respectively. Units are indicated in brackets within panels. Time since ZE refers years since the beginning of zero-emission.

We first computed the global mean of a diverse set of variables to examine the global scale temperature stabilization and the physical state that stems out of net-zero. Figure 2 shows the evolution of ΔGMCO2, ΔGMSAT, ΔGMSST, ΔRF, ΔOHU and their imbalance during the 02Kpd ramp-up and 300-years following CO_2-emission cessation relative to esm-piControl mean. In all net-zero simulations, GMCO2 declines exponentially resulting from the carbon-pump led by the land and ocean sinks,

https://doi.org/10.5194/egusphere-2026-993
Preprint. Discussion started: 17 March 2026

consistent with other models after net-zero (C. Jones et al., 2025; MacDougall et al., 2020) or CO_2 emission pulses (Joos et al., 2013; Zickfeld et al., 2021).

GMSAT shows a relatively good stabilization after net-zero (Fig. 2b), with the exception of 02Kpd-45 and 02Kpd-50 , which show a slight decline. Table 2 quantifies the Zero Emissions Commitment (ZEC) metric across time horizons. Despite the largest slopes for 02Kpd-45 and 02Kpd-50 (-0.012 °C per decade and -0.013 °C per decade respectively) they have a relatively small ZEC, as the run starts warmer than the expected GWL, and then the decline balances through the second half of the run being colder. In this high-warming climate states, this feature is due to the ocean inertia to take up most of the energy imbalance due to the important accumulation of CO_2 into the atmosphere during the first decades. Experiments 02Kpd-11 and 02Kpd-15 show the largest ZEC due to sustained undershoot. Overall, ZEC are well constrained within the 0.4 °C range expected for 20 years transient GWL.

Table 2. GMSAT anomaly relative to the first year of the net-zero experiments and averaged over 21-year periods centered around the 25th, 50th, 290th and whole time series for ZEC_{25}, ZEC_{50}, ZEC_{290} and ZEC respectively. The last column indicates the slopes of each time series.

Experiment ID	ZEC_{25} [°C]	ZEC_{50} [°C]	ZEC_{290} [°C]	ZEC [°C]	Slope [°C per century]
02Kpd-11	-0.32	-0.35	-0.42	-0.36	-0.05
02Kpd-15	-0.13	-0.10	-0.24	-0.14	-0.03
02Kpd-20	-0.04	0.01	-0.05	-0.06	-0.01
02Kpd-25	-0.03	-0.02	-0.14	-0.02	-0.03
02Kpd-30	0.11	0.08	-0.02	0.10	-0.03
02Kpd-35	0.00	0.06	-0.00	0.01	-0.02
02Kpd-40	0.15	0.19	0.15	0.17	-0.00
02Kpd-45	0.08	0.12	-0.24	-0.04	-0.12
02Kpd-50	0.18	0.10	-0.22	-0.03	-0.13

GMSST follows similar stabilization and a decline for the two highest GWL net-zero runs after ~ 200 years of net-zero (Fig. 2c). High warming levels may be subjected to caveats from centennial cooling in 02Kpd-45 and 02Kpd-50 preventing the model from full stabilization, though less pronounced than for GMSAT.

https://doi.org/10.5194/egusphere-2026-993
Preprint. Discussion started: 17 March 2026

After emission cessation, decreasing atmospheric CO_2 concentration (Fig. 2a) reduces radiative forcing (Fig. 2d) resulting in a cooling effect of GMSAT, while decreasing ocean heat uptake leads to a warming effect (Fig. 2e). Figure 2f shows balance between these two effects for the first six net-zero simulations, but negative imbalance for 02Kpd-40 up to 02Kpd-50. This imbalance explains the negative slopes observed for 02Kpd-45 and 02Kpd-50 (Table 2).

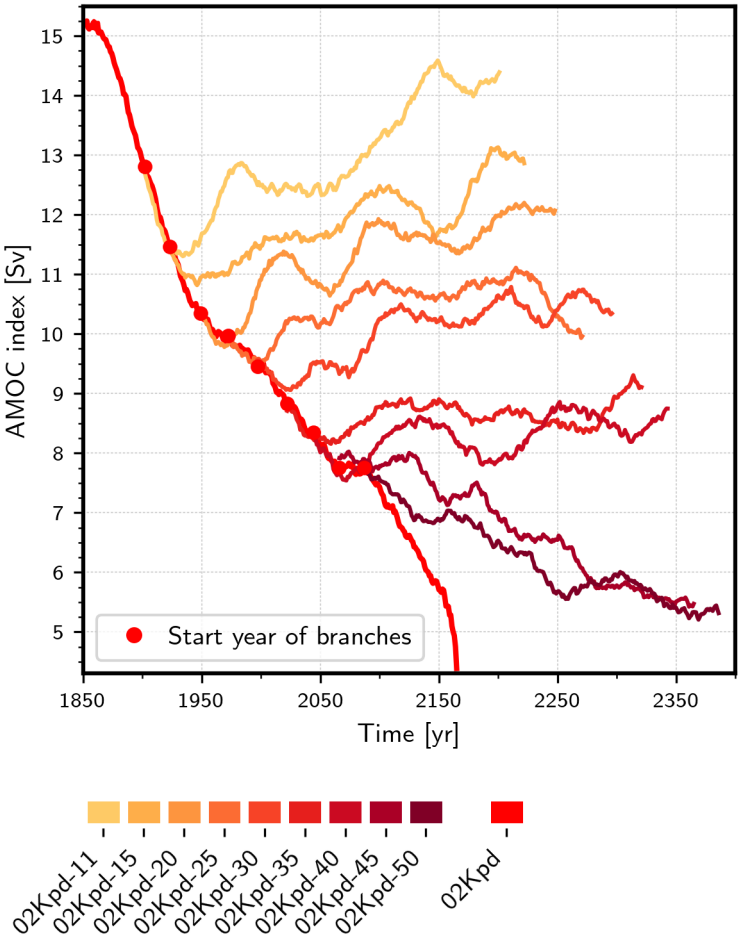

Figure 3. Atlantic meridional overturning circulation (AMOC) behaviour under net-zero. AMOC transport index calculated as the maximum of the AMOC streamfunction at 26 °N expressed in sverdrup (Sv) as a function of time. Colors grading from yellow to dark red stand for the different net-zero runs. Time series are smoothed with a 31-day running-mean. The red curve is the +0.2 °C per decade ramp-up simulation with corresponding round markers showing the years where net-zero runs start.

As an explanation of these responses, Fig. 3 shows the AMOC evolution during ramp-up and stabilization.CNRM-ESM2-2 shows the AMOC is declining with warming but shows recovery a few decades after temperature stabilization within a range of +1.1 °C and +3.0 °C. For instance, from the beginning of the ramp-up (1850-1870) until the first branch (1892-1912), the AMOC declines from 15.10 Sv to 12.80 Sv (-15.23 %). Following the +1.1 °C pathway, it keeps on decreasing to a minimum of 11.30 Sv in 1934. Then, the AMOC starts recovering by 26 %, reaching 14.26 Sv by the end of the net-zero run

https://doi.org/10.5194/egusphere-2026-993
Preprint. Discussion started: 17 March 2026

(2181-2201). Recovery weakens for GWL +3.5 °C and +4.0 °C. Above +4.0 °C, the AMOC declines persistently even after emissions are brought to zero.

For global warming levels above +4.0 °C, AMOC-SST correlations highlight a clear inter-hemispheric asymmetry (Fig. 4i-j) where SST declines with AMOC in the Northern Ocean domain (subpolar gyre, in particular) while increases in the Southern ocean. This relationship directly echoes the weakening of the conveyor-belt northern to southern latitudes heat transport .

CNRM-ESM2-2 compares well to other models such as GFDL-ESM2M as used in Lacroix et al., (2024) showing a recovery of the AMOC during a +1.5 °C stabilization phase, and NorESM2-LM projecting a weakening of the AMOC during the ramp-up stage, followed by a stabilization in the first decades of the zero-emission phase leading to a recovery at a multi-centennial scale (Schwinger et al., 2022), including similar Northern latitude cooling patterns.

Although our model exhibits a shift in the circulation-warming space (8 Sv – 4.5 K, see Fig. 3b) that brings the AMOC towards a weaker state in spite of emission cessation, it is hard to conclude if passing only one of these thresholds would result in a similar behaviour of the AMOC. Multi-model ensembles and hosing experiments (Jackson et al., 2023) would be then required to answer this question and assess this potential tipping point of AMOC in the circulation-warming space.

https://doi.org/10.5194/egusphere-2026-993
Preprint. Discussion started: 17 March 2026

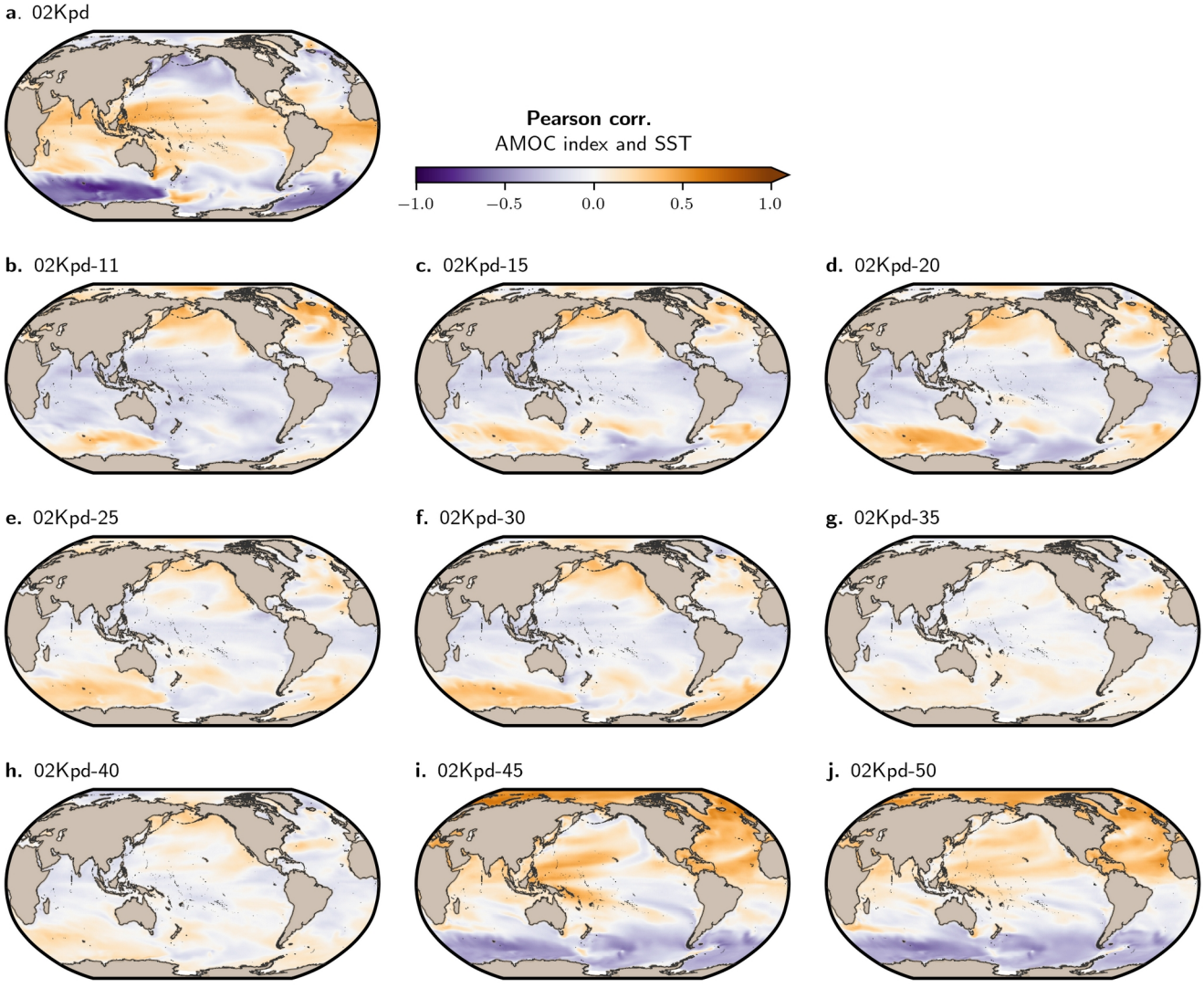

Figure 4. Correlation between the Atlantic meridional circulation (AMOC) index and the local sea surface temperature. Correlation expressed as the Pearson correlation coefficient for (a) the ramp-up run and (b-j) the 9 net-zero experiments. Orange (*resp.* purple) indicates positive (*resp.* negative) correlation.

Although the SST stabilizes quite well after emission cessation (see Fig. 2c) due to quick GMSAT equilibration, but sub-surface ocean temperatures take longer to reach equilibrium (Fig. 5 b). For instance, under the +2.0 °C GWL scenario, the exponential fit equilibrium timescale t_{90} is 38 years for the subsurface layer compared with 157 years for the deeper layer. Similarly, in the +5.0 °C GWL run, t_{90} remains on a decadal scale for the subsurface (21 years) while reaches centennial scales for the deeper layer (223 years).

https://doi.org/10.5194/egusphere-2026-993
Preprint. Discussion started: 17 March 2026

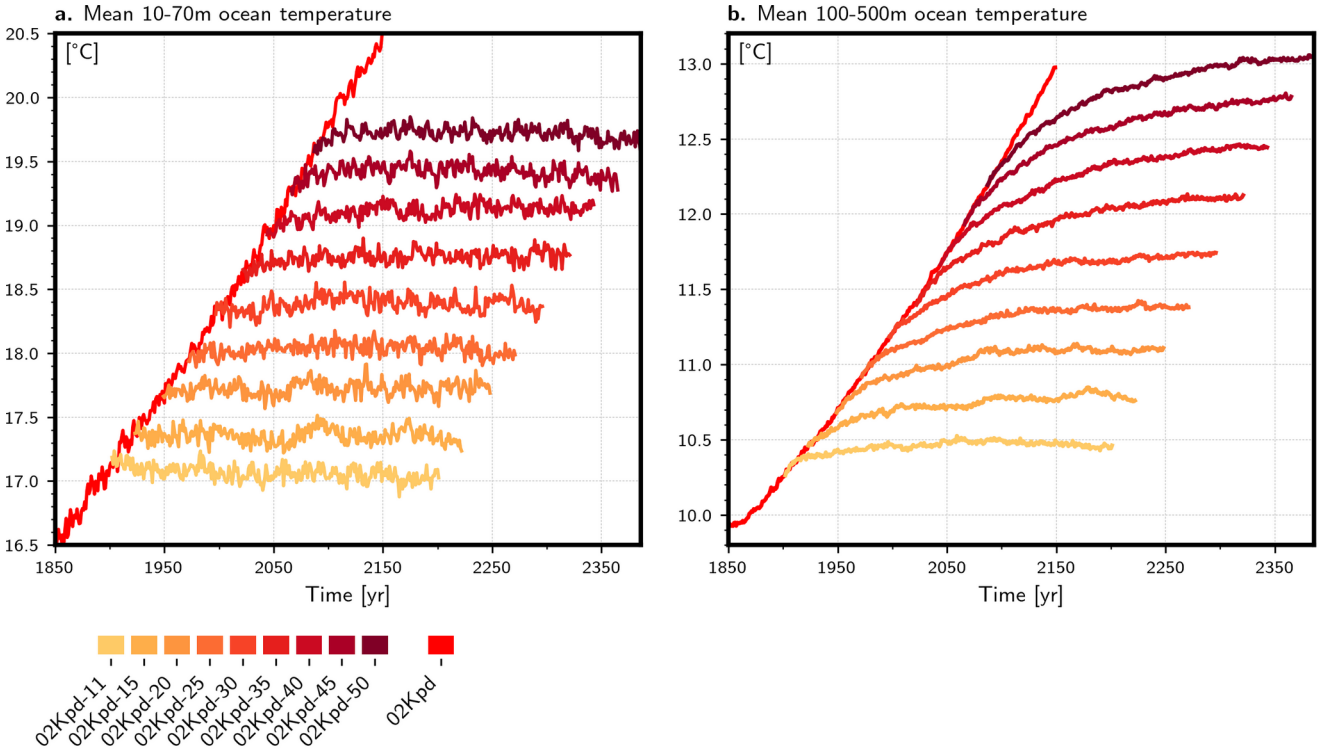

Figure 5. In-depth ocean temperature behaviour after net-zero. Global ocean temperature averaged in (a) the 10-70m and (b) 100-500m deep layers. Colors grading from yellow to dark red stand for the different net-zero runs. The red curve is the +0.2 °C per decade ramp-up simulation.

https://doi.org/10.5194/egusphere-2026-993
Preprint. Discussion started: 17 March 2026

3.2 SST anomaly distributions

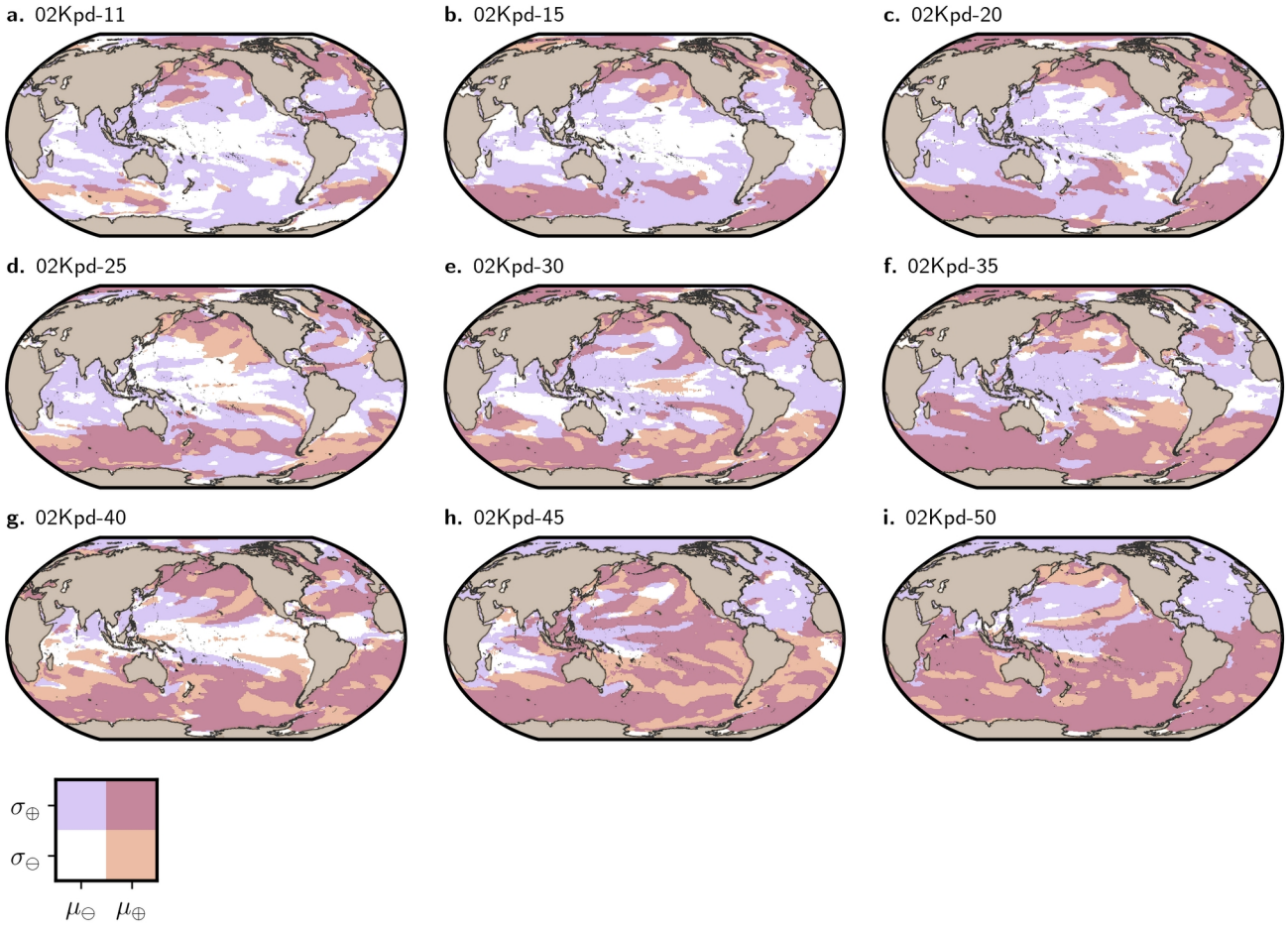

Figure 6. Regional changes in the mean and variance of the local SST anomaly distributions for the whole net-zero simulations relative to transient baselines. The maps highlight regions where the mean (μ) and (σ) the variance of SST distributions calculated over the whole net-zero simulations are increasing or decreasing relative to their respective transient baseline. Panels (a-i) decline the information for each net-zero run. Increases in the mean (*resp.* variance) only are shown in orange (*resp.* purple). Co-occurring increases (*resp.* decreases) in both the mean and variance are shown in red (*resp.* white). The color scheme is summarized by the bivariate color map.

This section compares local SST anomalies between stabilized and transient climates by analysing changes in their first two statistical moments: the mean (μ) and the standard deviation (σ). According to Vasseur et al., (2014), changes in variance and skewness can impact species more strongly than shifts in temperature mean, which has yet been the preferential statistic in impact studies.

Figure 6 maps regional anomalies of μ and σ averaged over the whole net-zero run for each GWL. A bivariate color map distinguishes co-occurring decreases (white, $\mu\ominus;\sigma\ominus$), co-occurring increases (red, $\mu\oplus;\sigma\oplus$), and opposing changes (purple and orange , $\mu\ominus;\sigma\oplus$ and $\mu\oplus;\sigma\ominus$). Regions where changes are not statistically significant according to a Kolmogorov-

https://doi.org/10.5194/egusphere-2026-993
Preprint. Discussion started: 17 March 2026

Smirnov test are scarce, accounting only about 1 % of the global ocean above +3.0 °C GWL, thus they are not visible on the maps. Welch and Levene statistical t-tests for single μ or σ changes are provided in Fig. S1 and Fig. S2 respectively.

Figure 7 summarizes the global ocean area of these four cases. Joint increases expand from covering 20 % of the global ocean in 02Kpd-11 to up to 67 % in the highest GWL stabilization scenario. On the other hand, no clear behaviour is found in the relationship between GWL and the fractional areas where only variance is increasing (purple bar). Regions where both mean and variance decrease with global warming, going from 33 % for 02Kpd-11 to only 3 % in 02Kpd-50.

These global tendencies depend on the time horizons and periods considered. During the early stable period, μ⊕ regions shows larger areas as a consequence of recent warming (Fig. S3a). Nevertheless, the relationship between μ⊕ area and GWL is less pronounced for the 300 years after emission cestion. (Fig. S3b).

Geographical patterns stand out in Fig. 6. Compound increases (μ⊕;σ⊕) concentrate mostly at high latitudes and progressively expand towards the tropics as GWL rises from +1.1 °C to +4.0 °C, while above that GWL, they concentrate in the Southern hemisphere. In the Southern Ocean, a +1.1 °C to +1.5 °C increase leads to a basin-wide increase in variability, while half of the region also endures an increase in the mean. In the early stable period, all basins feature higher μ and σ than in the transient baseline, with increasingly heterogeneous patterns as global warming intensifies (Fig. S4). In comparison, the late stable period resembles the whole net-zero time series (Fig. S5).

https://doi.org/10.5194/egusphere-2026-993
Preprint. Discussion started: 17 March 2026

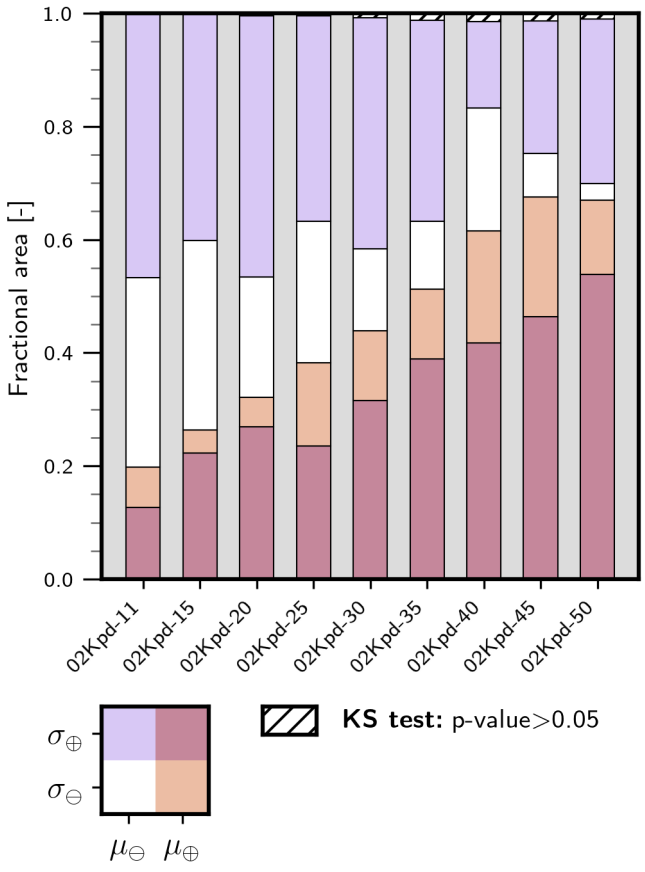

310 **Figure 7. Fractions of the global ocean facing single or compound increases in the mean or variance of the SST distributions over the whole net-zero simulations. Each bar sums up the information for each net-zero run. Increases in the mean (*resp.* variance) only are shown in orange (*resp.* purple). Co-occurring increases (*resp.* decreases) in both the mean and variance are shown in red (*resp.* white). The color scheme is summarized by the bivariate color map. Hatching indicates the fraction of the ocean where changes are not deemed significant judging by the result of a Kolmogorov-Smirnov statistical test.**

https://doi.org/10.5194/egusphere-2026-993
Preprint. Discussion started: 17 March 2026

315 **3.3 Emerging features of MHW in stabilized climate**

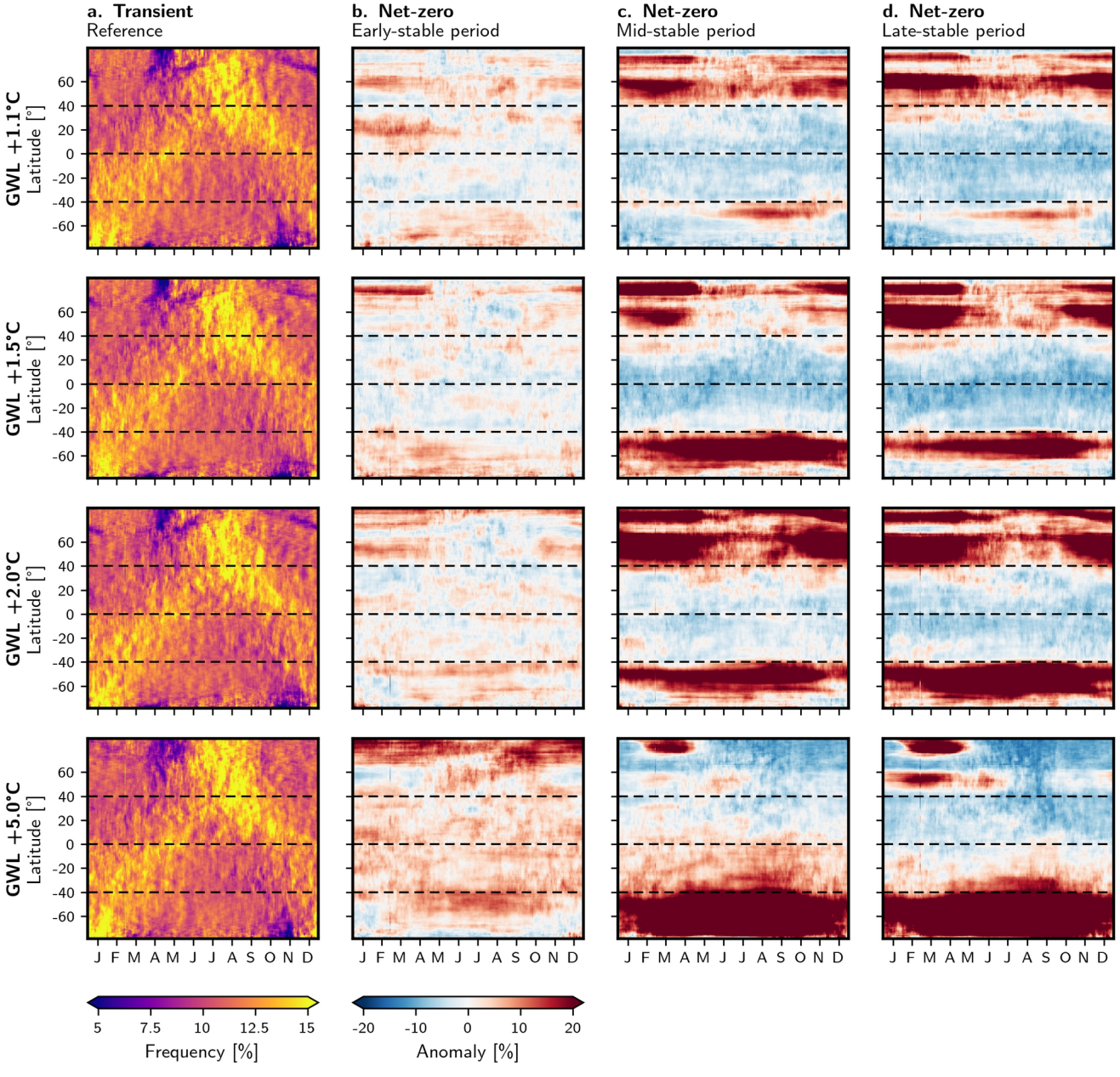

Figure 8. Seasonal cycle of marine heatwaves frequency and projected absolute anomalies. Each line of panels stands for a given net-zero run stabilizing the global climate around the following global warming levels (GWL) : +1.1 °C, +1.5 °C, +2.0 °C and +5.0 °C. (a) The first column indicates the seasonal cycle of the zonal mean MHW frequency over the TWL period. (b-d) Following columns give the projected absolute anomalies in the net-zero runs for the early-, mid- and late-stable periods relative to the TWL 320 **period. Red stands for higher frequency of MHW in net-zero whereas blue indicates a lower frequency than in the transient framework.**

https://doi.org/10.5194/egusphere-2026-993
Preprint. Discussion started: 17 March 2026

Building on SST anomaly distribution changes, we now focus on the evolution of the frequency and intensity of marine temperature extremes, i.e., marine heatwaves (MHW) against transient baselines.

Figure 8 shows the zonal mean seasonal MHW frequency for selected GWL (+1.1 °C, +1.5 °C, +2.0 °C and +5.0 °C relative to the pre-industrial mean state). Column (a) presents transient baselines. Columns (b-d) show net zero absolute anomalies for early stable (0-20 years), mid stable (140-160 years) and late stable (280-300 years) periods after emission cessation. Results for relative anomalies are shown in Fig. S6.

Early-stable periods remain quite close to the transient mean state, but mid- and late-stable periods display more abrupt changes (Fig. 8). During these periods, MHW frequency intensifies in the northern and southern extratropics bands (higher than 40 °N/°S) where both mean and variability increased (Fig. 6 and Fig. S5), during the full seasonal cycle at higher than +1.1 °C GWL. In the northern hemisphere, the amplification peaks in winter for high GWL but persists all year long in the +1.1 °C stabilization simulation. Conversely, mid latitudes (40 °S to 40 °N) show consistent MHW frequency declines. These differences between (i) late and early stable periods and (ii) the late stable and transient baseline highlights long term temporal evolution and geographical redistribution of MHW occurrence throughout the stabilization framework, which are absent from transient frameworks.

https://doi.org/10.5194/egusphere-2026-993
Preprint. Discussion started: 17 March 2026

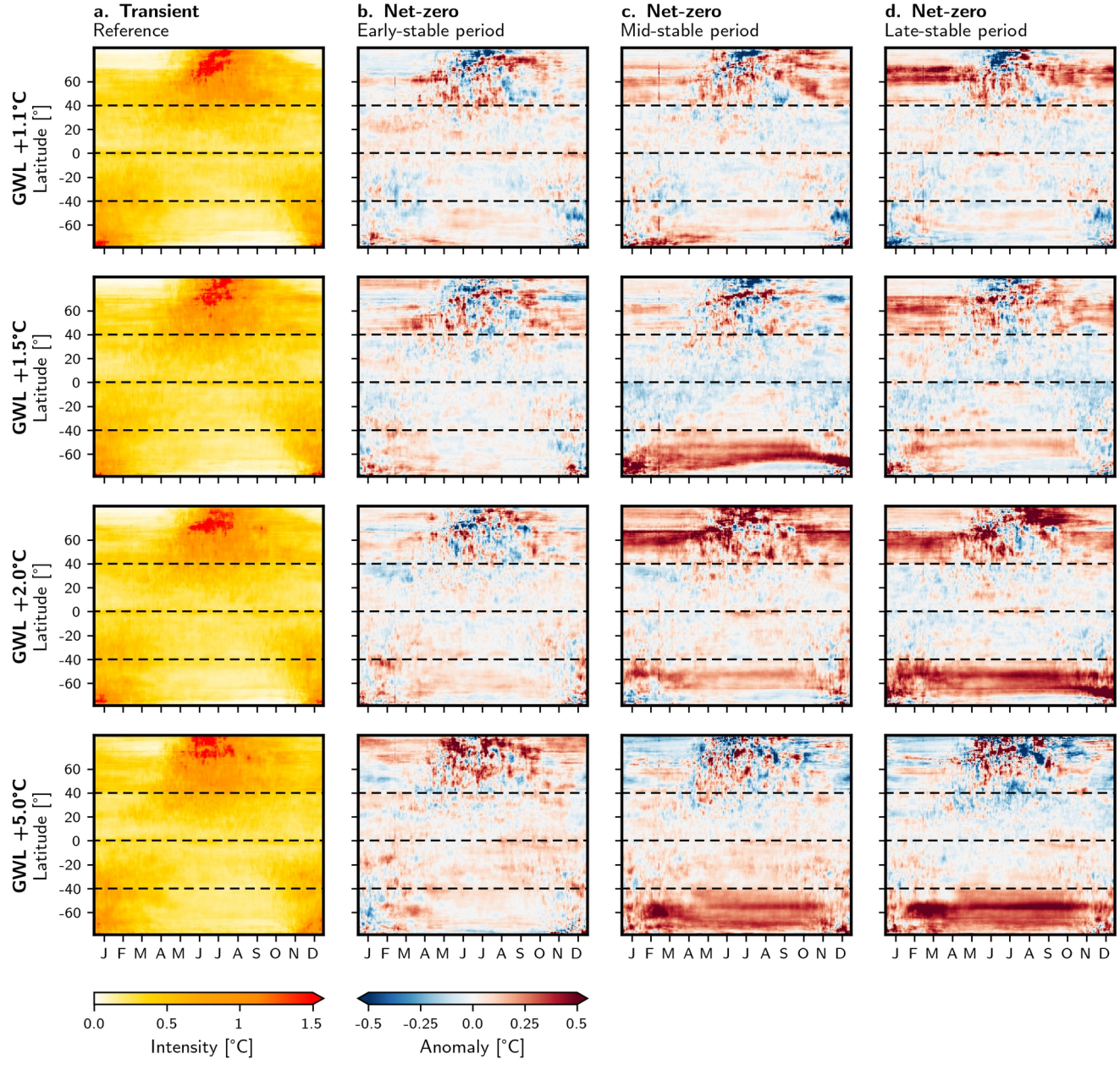

Figure 9. Seasonal cycle of marine heatwaves intensity and projected absolute anomalies. Each line of panels stands for a given net-zero run stabilizing the global climate around the following global warming levels (GWL) : +1.1 °C, +1.5 °C, +2.0 °C and +5.0 °C. (a) The first column indicates the seasonal cycle of the zonal mean MHW intensity over the TWL period. (b-d) Following columns give the projected absolute anomalies in the net-zero runs for the early-, mid- and late-stable periods relative to the TWL period. Red stands for higher intensity of MHW in net-zero whereas blue indicates a lower intensity than in the transient framework.

https://doi.org/10.5194/egusphere-2026-993
Preprint. Discussion started: 17 March 2026

Figure 9 mirrors the structure of Fig. 8 for MHW intensity (see Fig. S7 for relative anomalies). During the early-stable period, MHW intensity shows globally no clear geographical differences with the transient baseline. Under sustained net-zero emissions, the mid-latitudes also show stable MHW intensity throughout time and patterns of anomalies remain similar both geographically and temporally. Localized increases and decreases in intensity emerge within the northern latitudinal band (above 40 °N) during summer across all net-zero simulations. Runs exceeding +1.1 °C display relative mean increases above 100 % (Fig. S7), particularly from spring to autumn in the Southern Ocean and during winter at northern latitudes.

To better characterise the temporal evolution of MHW frequency and intensity, Fig. 10 quantifies the temporal evolution of Pearson correlations between zonal early stable seasonal cycles and those from fifteen successive 21-year periods in the net-zero simulations. For both MHW intensity (Fig. 10a) and frequency (Fig. 10b), as the seasonal cycle departs from the early stable state, the Pearson correlation coefficient decreases from 1. Intensity correlations remain high throughout stabilization, indicating persistent and coherent seasonal patterns across all periods. In contrast, frequency departs rapidly from the early stable pattern, followed by a lower but stable correlation after year 30 for all net-zero simulations. In several net-zero runs (+3.0 °C, +4.5 °C, and +5.0 °C), frequency even becomes anticorrelated suggesting pronounced changes in MHW characteristics. Overall, these results indicate no regime shift in intensity, and a rapid reorganization in frequency after emission cessation.

https://doi.org/10.5194/egusphere-2026-993
Preprint. Discussion started: 17 March 2026

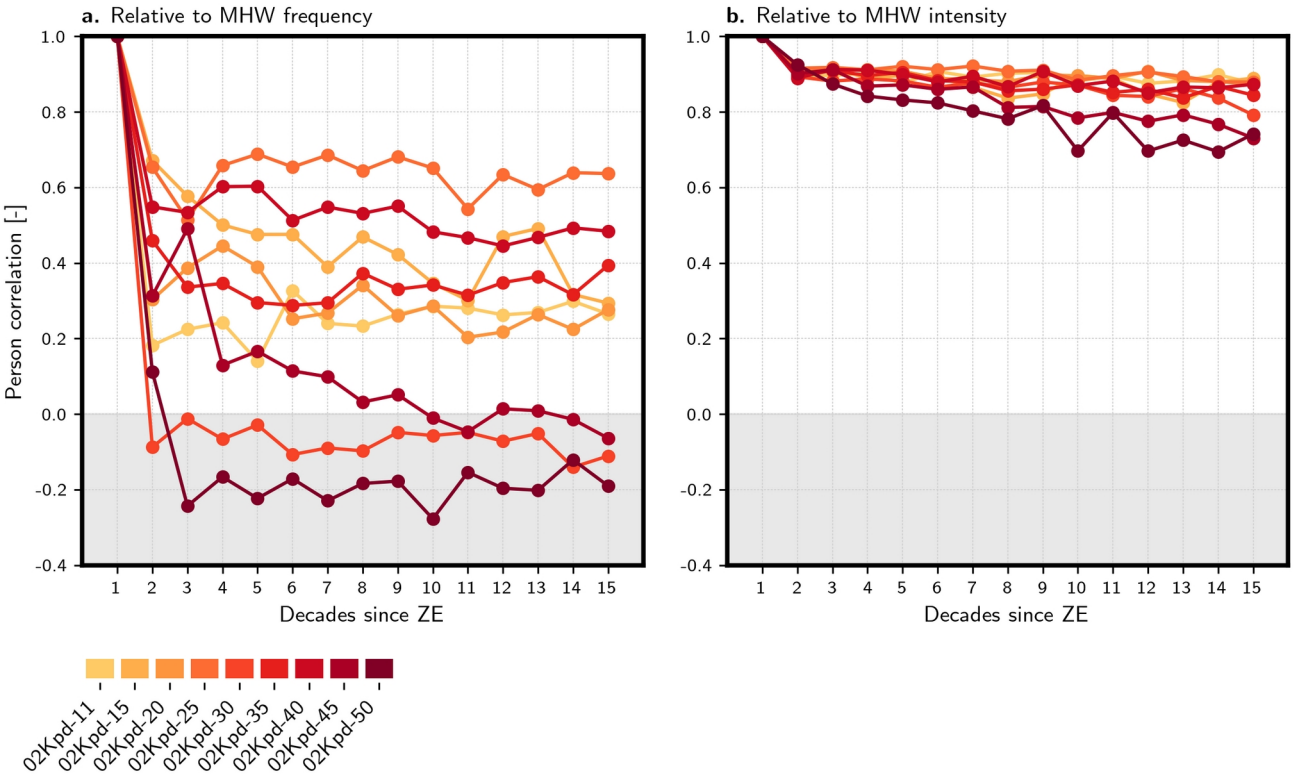

Figure 10. Correlations of daily zonal-mean seasonal cycles of marine heatwaves. Spatial Pearson correlation coefficient between the early-stable and each of the following 21-year windows plotted against the central decade index of each window. Correlations are computed from the daily zonal-mean seasonal cycle of (a) MHW frequency and (b) MHW intensity. Colors grading from yellow to red stand for the different net-zero runs. This figure illustrates how the seasonal cycle patterns diverge from the initial early state of stabilization as net-zero is on-going.

Stabilized climate MHW reveal striking decoupling between frequency and intensity. While occurrence redistributes towards high-latitudes, intensity remains comparatively stable without regime shift. This implies distinct mechanisms: frequency driven by threshold exceedance, which may differ in future climates, while intensity anchored by persistent background SST and heat accumulation.

High latitudes frequency increases together with mid-latitude decreases advocate for large-scale ocean heat reorganization. In particular, AMOC changes, and associated meridional heat redistribution, are likely to modulate regional SST variability and extremes (Ren & Liu, 2021), consistent with MHW frequency sensitivity to changes in the mean state and variance of SST(Capotondi et al., 2024; Frölicher et al., 2018; Xu et al., 2022).

By contrast, stable intensity suggests a steady or stronger local to regional forcings controlled by upper-ocean processes and air-sea heat fluxes (Holbrook et al., 2019; Sen Gupta et al., 2020). Rising upper-ocean stratification projected ocean wide

https://doi.org/10.5194/egusphere-2026-993
Preprint. Discussion started: 17 March 2026

(Cheng et al., 2022; Sallée et al., 2021) likely reduces vertical heat exchange, and heat accumulation; and may explain the persistence of a stable seasonal intensity pattern.

Internal variability through both remote drivers (e.g. El Nino Southern Oscillation, Indian Ocean Dipole; Holbrook et al., 2019) or regional modes (e.g. North Atlantic Oscillation, Guinaldo et al., 2025) also contribute to the spatially heterogeneous and seasonally dependent responses.

Limitations of single member approaches, like the present study, preclude process attribution. Large ensembles must thus quantify circulation adjustments, air-sea fluxes, upper-ocean stratification and changes in internal atmospheric and oceanic variability roles. Such ensembles are also essential to robustly sample internal climate variability and isolate the forced signals from stochastic fluctuations (Murphy et al., 2004; Tebaldi & Knutti, 2007). Large ensembles are necessary to assess the robustness of projected extremes, quantify event likelihoods, and identify plausible high-impact outliers (Atkins et al., 2025). Sampling these low-probability, high-impact extremes is a prerequisite for estimating return levels and supporting climate-risk assessments and adaptation planning, unachievable with single or small ensembles.

4 Conclusion

This study reveals the response of the ocean to multiple global warming levels stabilization following CO_2 emissions cessation. We generated nine 300-year simulations in which the global climate stabilizes across incremental levels of global warming ranging from +1.1 °C to +5.0 °C, using the CNRM-ESM2-2 coupled Earth system model.

Up to +4 °C of stabilization, CNRM-ESM2-2 simulates near-stable global mean surface air temperature over several centuries when the CO_2 emissions are brought to zero. Over this range of global warming, our results are comparable with those found by King et al., (2024) for multiple global warming levels ranging from +1.6 °C to +3.3 °C. The major difference is found for global warming targets strictly higher than +4.0 °C where CNRM-ESM2-2 exhibits a cooling of approximately -0.1 °C per century, due to ocean and climate feedbacks. This result contrasts with the warming trends found by King et al., (2024) and hence underscore the need to explore higher warming states as suggested in (C. Jones et al., 2025).

We were also capable of tracking changes in ocean surface properties through time, and found noticeable changes in SST across all the centennial-long simulations. These changes respond not only to changes in ocean circulation but to shifts in the capture and redistribution of absorbed heat across time.

As a direct consequence of SST changes, marine heatwaves reorganize poleward in all net-zero CO_2 emission simulations, with a frequency decreasing during stabilization in the mid-latitudes and tropics compared to high latitudes, where it largely raises. The intensity of MHW shows no clear tendency in the mid-latitudes and tropics whereas it increases in the Southern ocean during the spring to automn period. Our model suggests that the shift in frequency is taking place 30 years after stopping CO_2 emissions across all global warming levels.

https://doi.org/10.5194/egusphere-2026-993
Preprint. Discussion started: 17 March 2026

This finding also highlights that the standard 20-year period used to compute global warming level metrics could potentially undermine the magnitude of the impact in some regions.

Results presented in this study were obtained from just a single realisation of one Earth system model. To assess uncertainty of the response of the ocean to multiple net-zero CO_2 emissions contexts, ensemble or multi-model simulations could be relevant. Such work is planned in the context of TipMIP (C. Jones et al., 2025) where multiple models simulations will explore the climate response to CO_2 emission cessation where crossing +2.0 °C and +4.0 °C global warming levels.

Despite single model limitations, the general behaviour of CNRM-ESM2-2 compares well to other models such as GFDL-ESM2M (Lacroix et al., 2024) or NorESM2-LM (Schwinger et al., 2022), supporting the robustness of our stabilization responses.

Larger ensembles and multimodel studies are thus needed to robustly quantify uncertainty in regional SST responses, marine heatwave changes, and their impacts to marine ecosystems. Standard transient global warming levels approaches tend to hide frequency shifts and the regional redistribution of extremes that emerge decades after CO_2 emission cessation, leading to underestimation of their impacts. Our findings underscore that stabilized climate simulations are essential for impact assessments at targeted warming levels, as they capture relevant geophysical information of slow-adjusting ocean variables.

Code and data availability

Python scripts and data required to reproduce the figures of this paper are available at https://zenodo.org/records/18799136 (Bossert, 2026). The data can be direct outputs of the model or processed data.

Author contributions

IB and RS conceived the study and designed the modelling experiments. IB wrote the paper with text contributions and critical revisions from RS, YSF and TG. IB made the analyses and figures. IB performed the ramp-up and net-zero runs. RS performed the esm-piControl run.

Competing interests

The authors declare that they have no conflict of interest.

https://doi.org/10.5194/egusphere-2026-993
Preprint. Discussion started: 17 March 2026

Acknowledgements

We particularly acknowledge the support of the team in charge of the CNRM-CM climate model. Supercomputing time was provided by the Météo-France/DSI supercomputing center. We also acknowledge the French national Research Infrastructure CLIMERI-France (https://climeri-france.fr/) that provides support on modelling workflow, infrastructure and standards. R.S., received support from the European Union's Horizon 2020 research and innovation programme under Grant Agreement N° 101003536 (ESM2025—Earth System Models for the Future). R.S. also acknowledges funding from the European Union's Horizon Europe research and innovation programme under OptimESM (grant agreement No 101081193). This study has also received funding from Agence Nationale de la Recherche - France 2030 as part of the PEPR TRACCS programme under grant number ANR-22-EXTR-0008 and ANR-22-EXTR-0009.

References

Amaya, D. J., Jacox, M. G., Fewings, M. R., Saba, V. S., Stuecker, M. F., Rykaczewski, R. R., Ross, A. C., Stock, C. A., Capotondi, A., Petrik, C. M., Bograd, S. J., Alexander, M. A., Cheng, W., Hermann, A. J., Kearney, K. A., & Powell, B. S. (2023). Marine heatwaves need clear definitions so coastal communities can adapt. *Nature*, *616*(7955), 29-32. https://doi.org/10.1038/d41586-023-00924-2

Arora, V. K., Katavouta, A., Williams, R. G., Jones, C. D., Brovkin, V., Friedlingstein, P., Schwinger, J., Bopp, L., Boucher, O., Cadule, P., Chamberlain, M. A., Christian, J. R., Delire, C., Fisher, R. A., Hajima, T., Ilyina, T., Joetzjer, E., Kawamiya, M., Koven, C. D., … Ziehn, T. (2020). Carbon–concentration and carbon–climate feedbacks in CMIP6 models and their comparison to CMIP5 models. *Biogeosciences*, *17*(16), 4173-4222. https://doi.org/10.5194/bg-17-4173-2020

Atkins, J. R. C., Scaife, A. A., Graham, J. A., Tinker, J., & Halloran, P. R. (2025). Recent European marine heatwaves are unprecedented but not unexpected. *Communications Earth & Environment*, *6*(1), 792. https://doi.org/10.1038/s43247-025-02802-3

Aumont, O., Ethé, C., Tagliabue, A., Bopp, L., & Gehlen, M. (2015). PISCES-v2 : An ocean biogeochemical model for carbon and ecosystem studies. *Geoscientific Model Development*, *8*(8), 2465-2513. https://doi.org/10.5194/gmd-8-2465-2015

Benjamini, Y., & Hochberg, Y. (1995). Controlling the False Discovery Rate : A Practical and Powerful Approach to Multiple Testing. *Journal of the Royal Statistical Society: Series B (Methodological)*, *57*(1), 289-300. https://doi.org/10.1111/j.2517-6161.1995.tb02031.x

Bernard, B., Madec, G., Penduff, T., Molines, J.-M., Treguier, A.-M., Le Sommer, J., Beckmann, A., Biastoch, A., Böning, C., Dengg, J., Derval, C., Durand, E., Gulev, S., Remy, E., Talandier, C., Theetten, S., Maltrud, M., McClean, J., & De

https://doi.org/10.5194/egusphere-2026-993
Preprint. Discussion started: 17 March 2026

Cuevas, B. (2006). Impact of partial steps and momentum advection schemes in a global ocean circulation model at eddy-permitting resolution. *Ocean Dynamics*, *56*(5), 543-567. https://doi.org/10.1007/s10236-006-0082-1

Berthet, S., Jouanno, J., Séférian, R., Gehlen, M., & Llovel, W. (2023). How does the phytoplankton–light feedback affect the marine N_2O inventory? *Earth System Dynamics*, *14*(2), 399-412. https://doi.org/10.5194/esd-14-399-2023

Bossert, I., Baur, S., Cussac, M., & others. (2025). CNRM-ESM2-2 : Development and Evaluation of an Updated Version of the CNRM-CERFACS Earth System Model. *ESS Open Archive*. https://doi.org/10.22541/essoar.175977424.42948487/v1

Bossert, I. (2026). Ocean and marine heatwaves responses to multiple net-zero worlds - datasets and scripts for Figures 1 to 10 [Data set]. Zenodo. https://doi.org/10.5281/zenodo.18799136

Brown, M. B., & Forsythe, A. B. (1974). Robust Tests for the Equality of Variances. *Journal of the American Statistical Association*, *69*(346), 364-367. https://doi.org/10.1080/01621459.1974.10482955

Canadell, J. G., Monteiro, P. M. S., Costa, M. H., Cotrim da Cunha, L., Cox, P. M., Eliseev, A. V., Henson, S., Ishii, M., Jaccard, S., Koven, C., Lohila, A., Patra, P. K., Piao, S., Rogelj, J., Syampungani, S., Zaehle, S., & Zickfeld, K. (2021). Global Carbon and other Biogeochemical Cycles and Feedbacks. In V. Masson-Delmotte, P. Zhai, A. Pirani, S. L. Connors, C. Péan, S. Berger, N. Caud, Y. Chen, L. Goldfarb, M. I. Gomis, M. Huang, K. Leitzell, E. Lonnoy, J. B. R. Matthews, T. K. Maycock, T. Waterfield, O. Yelekçi, R. Yu, & B. Zhou (Éds.), *Climate Change 2021 : The Physical Science Basis* (p. 673-816). Cambridge University Press. https://doi.org/10.1017/9781009157896.007

Capotondi, A., Rodrigues, R. R., Sen Gupta, A., Benthuysen, J. A., Deser, C., Frölicher, T. L., Lovenduski, N. S., Amaya, D. J., Le Grix, N., Xu, T., Hermes, J., Holbrook, N. J., Martinez-Villalobos, C., Masina, S., Roxy, M. K., Schaeffer, A., Schlegel, R. W., Smith, K. E., & Wang, C. (2024). A global overview of marine heatwaves in a changing climate. *Communications Earth & Environment*, *5*(1), 701. https://doi.org/10.1038/s43247-024-01806-9

Cheng, L., Von Schuckmann, K., Abraham, J. P., Trenberth, K. E., Mann, M. E., Zanna, L., England, M. H., Zika, J. D., Fasullo, J. T., Yu, Y., Pan, Y., Zhu, J., Newsom, E. R., Bronselaer, B., & Lin, X. (2022). Past and future ocean warming. *Nature Reviews Earth & Environment*, *3*(11), 776-794. https://doi.org/10.1038/s43017-022-00345-1

Doney, S. C., Ruckelshaus, M., Emmett Duffy, J., Barry, J. P., Chan, F., English, C. A., Galindo, H. M., Grebmeier, J. M., Hollowed, A. B., Knowlton, N., Polovina, J., Rabalais, N. N., Sydeman, W. J., & Talley, L. D. (2012). Climate Change Impacts on Marine Ecosystems. *Annual Review of Marine Science*, *4*(1), 11-37. https://doi.org/10.1146/annurev-marine-041911-111611

Eyring, V., Bony, S., Meehl, G. A., Senior, C. A., Stevens, B., Stouffer, R. J., & Taylor, K. E. (2016). Overview of the Coupled Model Intercomparison Project Phase 6 (CMIP6) experimental design and organization. *Geoscientific Model Development*, *9*(5), 1937-1958. https://doi.org/10.5194/gmd-9-1937-2016

https://doi.org/10.5194/egusphere-2026-993
Preprint. Discussion started: 17 March 2026

Eyring, V., Gillett, N. P., Achuta Rao, K. M., Barimalala, R., Barreiro Parrillo, M., Bellouin, N., Cassou, C., Durack, P. J., Kosaka, Y., McGregor, S., Min, S.-K., Morgenstern, O., & Sun, Y. (2021). Human Influence on the Climate System. In V. Masson-Delmotte, P. Zhai, A. Pirani, S. L. Connors, C. Péan, S. Berger, N. Caud, Y. Chen, L. Goldfarb, M. I. Gomis, M. Huang, K. Leitzell, E. Lonnoy, J. B. R. Matthews, T. K. Maycock, T. Waterfield, O. Yelekçi, R. Yu, & B. Zhou (Éds.), *Climate Change 2021 : The Physical Science Basis* (p. 423-552). Cambridge University Press. https://doi.org/10.1017/9781009157896.005

Frölicher, T. L., Fischer, E. M., & Gruber, N. (2018). Marine heatwaves under global warming. *Nature*, *560*(7718), 360-364. https://doi.org/10.1038/s41586-018-0383-9

Gillett, N. P., Arora, V. K., Zickfeld, K., Marshall, S. J., & Merryfield, W. J. (2011). Ongoing climate change following a complete cessation of carbon dioxide emissions. *Nature Geoscience*, *4*(2), 83-87. https://doi.org/10.1038/ngeo1047

Guinaldo, T., Cassou, C., Sallée, J.-B., & Liné, A. (2025). Internal variability effect doped by climate change drove the 2023 marine heat extreme in the North Atlantic. *Communications Earth & Environment*, *6*(1), 291. https://doi.org/10.1038/s43247-025-02197-1

Guinaldo, T., & Neukermans, G. (2026). Compounded effects of long-term warming and the exceptional 2023 marine heatwave on North Atlantic coccolithophore bloom dynamics. *Ocean Science*, *22*(1), 145-166. https://doi.org/10.5194/os-22-145-2026

Hobday, A. J., Alexander, L. V., Perkins, S. E., Smale, D. A., Straub, S. C., Oliver, E. C. J., Benthuysen, J. A., Burrows, M. T., Donat, M. G., Feng, M., Holbrook, N. J., Moore, P. J., Scannell, H. A., Sen Gupta, A., & Wernberg, T. (2016). A hierarchical approach to defining marine heatwaves. *Progress in Oceanography*, *141*, 227-238. https://doi.org/10.1016/j.pocean.2015.12.014

Holbrook, N. J., Scannell, H. A., Sen Gupta, A., Benthuysen, J. A., Feng, M., Oliver, E. C. J., Alexander, L. V., Burrows, M. T., Donat, M. G., Hobday, A. J., Moore, P. J., Perkins-Kirkpatrick, S. E., Smale, D. A., Straub, S. C., & Wernberg, T. (2019). A global assessment of marine heatwaves and their drivers. *Nature Communications*, *10*(1), 2624. https://doi.org/10.1038/s41467-019-10206-z

Jones, C., Bossert, I., Dennis, D. P., Jeffery, H., Jones, C. D., Koenigk, T., Loriani, S., Sanderson, B., Séférian, R., Wyser, K., Yang, S., Abe, M., Bathiany, S., Braconnot, P., Brovkin, V., Burger, F. A., Cadule, P., Castruccio, F. S., Danabasoglu, G., … Ziehn, T. (2025). The TIPMIP Earth system model experiment protocol : Phase 1. *EGUsphere*, 1-45. https://doi.org/10.5194/egusphere-2025-3604

Jones, C. D., Frölicher, T. L., Koven, C., MacDougall, A. H., Matthews, H. D., Zickfeld, K., Rogelj, J., Tokarska, K. B., Gillett, N. P., Ilyina, T., Meinshausen, M., Mengis, N., Séférian, R., Eby, M., & Burger, F. A. (2019). The Zero Emissions

https://doi.org/10.5194/egusphere-2026-993
Preprint. Discussion started: 17 March 2026

Commitment Model Intercomparison Project (ZECMIP) contribution to C4MIP : Quantifying committed climate changes following zero carbon emissions. *Geoscientific Model Development*, *12*(10), 4375-4385. https://doi.org/10.5194/gmd-12-4375-2019

Joos, F., Roth, R., Fuglestvedt, J. S., Peters, G. P., Enting, I. G., von Bloh, W., Brovkin, V., Burke, E. J., Eby, M., Edwards, N. R., Friedrich, T., Frölicher, T. L., Halloran, P. R., Holden, P. B., Jones, C., Kleinen, T., Mackenzie, F. T., Matsumoto, K., Meinshausen, M., … Weaver, A. J. (2013). Carbon dioxide and climate impulse response functions for the computation of greenhouse gas metrics : A multi-model analysis. *Atmospheric Chemistry and Physics*, *13*(5), 2793-2825. https://doi.org/10.5194/acp-13-2793-2013

King, A. D., Karoly, D. J., & Henley, B. J. (2017). Australian climate extremes at 1.5 °C and 2 °C of global warming. *Nature Climate Change*, *7*(6), 412-416. https://doi.org/10.1038/nclimate3296

King, A. D., Ziehn, T., Chamberlain, M., Borowiak, A. R., Brown, J. R., Cassidy, L., Dittus, A. J., Grose, M., Maher, N., Paik, S., Perkins-Kirkpatrick, S. E., & Sengupta, A. (2024). Exploring climate stabilisation at different global warming levels in ACCESS-ESM-1.5. *Earth System Dynamics*, *15*(5), 1353-1383. https://doi.org/10.5194/esd-15-1353-2024

Lacroix, F., Burger, F. A., Silvy, Y., Schleussner, C.-F., & Frölicher, T. L. (2024). Persistently Elevated High-Latitude Ocean Temperatures and Global Sea Level Following Temporary Temperature Overshoots. *Earth's Future*, *12*(10), e2024EF004862. https://doi.org/10.1029/2024EF004862

Laufkötter, C., Zscheischler, J., & Frölicher, T. L. (2020). High-impact marine heatwaves attributable to human-induced global warming. *Science*, *369*(6511), 1621-1625. https://doi.org/10.1126/science.aba0690

Le Grix, N., Zscheischler, J., Laufkötter, C., Rousseaux, C. S., & Frölicher, T. L. (2021). Compound high-temperature and low-chlorophyll extremes in the ocean over the satellite period. *Biogeosciences*, *18*(6), 2119-2137. https://doi.org/10.5194/bg-18-2119-2021

MacDougall, A. H., Frölicher, T. L., Jones, C. D., Rogelj, J., Matthews, H. D., Zickfeld, K., Arora, V. K., Barrett, N. J., Brovkin, V., Burger, F. A., Eby, M., Eliseev, A. V., Hajima, T., Holden, P. B., Jeltsch-Thömmes, A., Koven, C., Mengis, N., Menviel, L., Michou, M., … Ziehn, T. (2020). Is there warming in the pipeline? A multi-model analysis of the Zero Emissions Commitment from CO_2. *Biogeosciences*, *17*(11), 2987-3016. https://doi.org/10.5194/bg-17-2987-2020

Madec, G., Bourdallé-Badie, R., Bouttier, P.-A., Bricaud, C., Bruciaferri, D., Calvert, D., Chanut, J., Clementi, E., Coward, A., Delrosso, D., Ethé, C., Flavoni, S., Graham, T., Harle, J., Iovino, D., Lea, D., Lévy, C., Lovato, T., Martin, N., … Vancoppenolle, M. (2017). *NEMO ocean engine*. https://doi.org/10.5281/zenodo.1472492

Massey Jr., F. J. (1951). The Kolmogorov-Smirnov Test for Goodness of Fit. *Journal of the American Statistical Association*, *46*(253), 68-78. https://doi.org/10.1080/01621459.1951.10500769

https://doi.org/10.5194/egusphere-2026-993
Preprint. Discussion started: 17 March 2026

Masson-Delmotte, V., Zhai, P., Pörtner, H.-O., Roberts, D., Skea, J., Shukla, P., Pirani, A., Moufouma-Okia, W., Péan, C., Pidcock, R., Connors, S., Matthews, J., Chen, Y., Zhou, X., Gomis, M., Lonnoy, E., Maycock, T., Tignor, M., & Waterfield, T. (2018). *Global Warming of 1.5° C. An IPCC Special Report on the Impacts of Global Warming of 1.5° C Above Pre-Industrial Levels and Related Global Greenhouse Gas Emission Pathways, in the Context of Strengthening the Global Response to the Threat of Climate Change*. IPCC. https://doi.org/10.1017/9781009157940

Mathiot, P., Jenkins, A., Harris, C., & Madec, G. (2017). Explicit representation and parametrised impacts of under ice shelf seas in the z^* coordinate ocean model NEMO 3.6. *Geoscientific Model Development*, *10*(7), 2849-2874. https://doi.org/10.5194/gmd-10-2849-2017

Matthews, H. D., & Wynes, S. (2022). Current global efforts are insufficient to limit warming to 1.5°C. *Science*, *376*(6600), 1404-1409. https://doi.org/10.1126/science.abo3378

Murphy, J. M., Sexton, D. M. H., Barnett, D. N., Jones, G. S., Webb, M. J., Collins, M., & Stainforth, D. A. (2004). Quantification of modelling uncertainties in a large ensemble of climate change simulations. *Nature*, *430*(7001), 768-772. https://doi.org/10.1038/nature02771

Myhre, G., Highwood, E. J., Shine, K. P., & Stordal, F. (1998). New estimates of radiative forcing due to well mixed greenhouse gases. *Geophysical Research Letters*, *25*(14), 2715-2718. https://doi.org/10.1029/98GL01908

Oliver, E. C. J., Benthuysen, J. A., Darmaraki, S., Donat, M. G., Hobday, A. J., Holbrook, N. J., Schlegel, R. W., & Sen Gupta, A. (2021). Marine Heatwaves. *Annual Review of Marine Science*, *13*(1), 313-342. https://doi.org/10.1146/annurev-marine-032720-095144

Palazzo Corner, S., Siegert, M., Ceppi, P., Fox-Kemper, B., Frölicher, T. L., Gallego-Sala, A., Haigh, J., Hegerl, G. C., Jones, C. D., Knutti, R., Koven, C. D., MacDougall, A. H., Meinshausen, M., Nicholls, Z., Sallée, J. B., Sanderson, B. M., Séférian, R., Turetsky, M., Williams, R. G., … Rogelj, J. (2023). The Zero Emissions Commitment and climate stabilization. *Frontiers in Science*, *1*. https://doi.org/10.3389/fsci.2023.1170744

Pörtner, H. O., & Farrell, A. P. (2008). Physiology and Climate Change. *Science*, *322*(5902), 690-692. https://doi.org/10.1126/science.1163156

Ren, X., & Liu, W. (2021). The Role of a Weakened Atlantic Meridional Overturning Circulation in Modulating Marine Heatwaves in a Warming Climate. *Geophysical Research Letters*, *48*(23), e2021GL095941. https://doi.org/10.1029/2021GL095941

Roehrig, R., Beau, I., Saint-Martin, D., Alias, A., Decharme, B., Guérémy, J.-F., Voldoire, A., Abdel-Lathif, A. Y., Bazile, E., Belamari, S., Blein, S., Bouniol, D., Bouteloup, Y., Cattiaux, J., Chauvin, F., Chevallier, M., Colin, J., Douville, H.,

https://doi.org/10.5194/egusphere-2026-993
Preprint. Discussion started: 17 March 2026

Marquet, P., … Sénési, S. (2020). The CNRM Global Atmosphere Model ARPEGE-Climat 6.3 : Description and Evaluation. *Journal of Advances in Modeling Earth Systems*, *12*(7), e2020MS002075. https://doi.org/10.1029/2020MS002075

Salas Mélia, D. (2002). A global coupled sea ice–ocean model. *Ocean Modelling*, *4*(2), 137-172. https://doi.org/10.1016/S1463-5003(01)00015-4

Sallée, J.-B., Pellichero, V., Akhoudas, C., Pauthenet, E., Vignes, L., Schmidtko, S., Garabato, A. N., Sutherland, P., & Kuusela, M. (2021). Summertime increases in upper-ocean stratification and mixed-layer depth. *Nature*, *591*(7851), 592-598. https://doi.org/10.1038/s41586-021-03303-x

Sanderson, B. M., Brovkin, V., Fisher, R. A., Hohn, D., Ilyina, T., Jones, C. D., Koenigk, T., Koven, C., Li, H., Lawrence, D. M., Lawrence, P., Liddicoat, S., MacDougall, A. H., Mengis, N., Nicholls, Z., O'Rourke, E., Romanou, A., Sandstad, M., Schwinger, J., … Ziehn, T. (2025). flat10MIP : An emissions-driven experiment to diagnose the climate response to positive, zero and negative CO_2 emissions. *Geoscientific Model Development*, *18*(17), 5699-5724. https://doi.org/10.5194/gmd-18-5699-2025

Santana-Falcón, Y., & Séférian, R. (2022). Climate change impacts the vertical structure of marine ecosystem thermal ranges. *Nature Climate Change*, *12*(10), 935-942. https://doi.org/10.1038/s41558-022-01476-5

Schwinger, J., Asaadi, A., Goris, N., & Lee, H. (2022). Possibility for strong northern hemisphere high-latitude cooling under negative emissions. *Nature Communications*, *13*(1), 1095. https://doi.org/10.1038/s41467-022-28573-5

Séférian, R., Nabat, P., Michou, M., Saint-Martin, D., Voldoire, A., Colin, J., Decharme, B., Delire, C., Berthet, S., Chevallier, M., Sénési, S., Franchisteguy, L., Vial, J., Mallet, M., Joetzjer, E., Geoffroy, O., Guérémy, J.-F., Moine, M.-P., Msadek, R., … Madec, G. (2019). Evaluation of CNRM Earth System Model, CNRM-ESM2-1 : Role of Earth System Processes in Present-Day and Future Climate. *Journal of Advances in Modeling Earth Systems*, *11*(12), 4182-4227. https://doi.org/10.1029/2019MS001791

Sen Gupta, A., Thomsen, M., Benthuysen, J. A., Hobday, A. J., Oliver, E., Alexander, L. V., Burrows, M. T., Donat, M. G., Feng, M., Holbrook, N. J., Perkins-Kirkpatrick, S., Moore, P. J., Rodrigues, R. R., Scannell, H. A., Taschetto, A. S., Ummenhofer, C. C., Wernberg, T., & Smale, D. A. (2020). Drivers and impacts of the most extreme marine heatwave events. *Scientific Reports*, *10*(1), 19359. https://doi.org/10.1038/s41598-020-75445-3

Silvy, Y., Frölicher, T. L., Terhaar, J., Joos, F., Burger, F. A., Lacroix, F., Allen, M., Bernardello, R., Bopp, L., Brovkin, V., Buzan, J. R., Cadule, P., Dix, M., Dunne, J., Friedlingstein, P., Georgievski, G., Hajima, T., Jenkins, S., Kawamiya, M., … Ziehn, T. (2024). AERA-MIP : Emission pathways, remaining budgets, and carbon cycle dynamics compatible with 1.5 and 2 °C global warming stabilization. *Earth System Dynamics*, *15*(6), 1591-1628. https://doi.org/10.5194/esd-15-1591-2024

https://doi.org/10.5194/egusphere-2026-993
Preprint. Discussion started: 17 March 2026

Smith, K. E., Burrows, M. T., Hobday, A. J., King, N. G., Moore, P. J., Sen Gupta, A., Thomsen, M. S., Wernberg, T., & Smale, D. A. (2023). Biological Impacts of Marine Heatwaves. *Annual Review of Marine Science*, *15*(1), 119-145. https://doi.org/10.1146/annurev-marine-032122-121437

Smith, K. E., Burrows, M. T., Hobday, A. J., Sen Gupta, A., Moore, P. J., Thomsen, M., Wernberg, T., & Smale, D. A. (2021). Socioeconomic impacts of marine heatwaves : Global issues and opportunities. *Science*, *374*(6566), eabj3593. https://doi.org/10.1126/science.abj3593

Tebaldi, C., & Knutti, R. (2007). The use of the multi-model ensemble in probabilistic climate projections. *Philosophical Transactions of the Royal Society A: Mathematical, Physical and Engineering Sciences*, *365*(1857), 2053-2075. https://doi.org/10.1098/rsta.2007.2076

Terhaar, J., Frölicher, T. L., Aschwanden, M. T., Friedlingstein, P., & Joos, F. (2022). Adaptive emission reduction approach to reach any global warming target. *Nature Climate Change*, *12*(12), Article 12. https://doi.org/10.1038/s41558-022-01537-9

Terhaar, J., Frölicher, T. L., & Joos, F. (2023). Ocean acidification in emission-driven temperature stabilization scenarios : The role of TCRE and non-CO2 greenhouse gases. *Environmental Research Letters*, *18*(2), 024033. https://doi.org/10.1088/1748-9326/acaf91

UNFCCC. (2015, décembre). *Adoption of the Paris Agreement*. https://unfccc.int/resource/docs/2015/cop21/eng/l09r01.pdf

Vasseur, D. A., DeLong, J. P., Gilbert, B., Greig, H. S., Harley, C. D. G., McCann, K. S., Savage, V., Tunney, T. D., & O'Connor, M. I. (2014). Increased temperature variation poses a greater risk to species than climate warming. *Proceedings of the Royal Society B: Biological Sciences*, *281*(1779), 20132612. https://doi.org/10.1098/rspb.2013.2612

von Schuckmann, K., Minière, A., Gues, F., Cuesta-Valero, F. J., Kirchengast, G., Adusumilli, S., Straneo, F., Ablain, M., Allan, R. P., Barker, P. M., Beltrami, H., Blazquez, A., Boyer, T., Cheng, L., Church, J., Desbruyeres, D., Dolman, H., Domingues, C. M., García-García, A., … Zemp, M. (2023). Heat stored in the Earth system 1960–2020 : Where does the energy go? *Earth System Science Data*, *15*(4), 1675-1709. https://doi.org/10.5194/essd-15-1675-2023

Welch, B. L. (1947). The generalization of « Student's » problem when several different population variances are involved. *Biometrika*, *34*(1-2), 28-35. https://doi.org/10.1093/biomet/34.1-2.28

Wernberg, T., Thomsen, M. S., Burrows, M. T., Filbee-Dexter, K., Hobday, A. J., Holbrook, N. J., Montie, S., Moore, P. J., Oliver, E. C. J., Sen Gupta, A., Smale, D. A., & Smith, K. (2025). Marine heatwaves as hot spots of climate change and impacts on biodiversity and ecosystem services. *Nature Reviews Biodiversity*, *1*(7), 461-479. https://doi.org/10.1038/s44358-025-00058-5

https://doi.org/10.5194/egusphere-2026-993
Preprint. Discussion started: 17 March 2026

Xu, T., Newman, M., Capotondi, A., Stevenson, S., Di Lorenzo, E., & Alexander, M. A. (2022). An increase in marine heatwaves without significant changes in surface ocean temperature variability. *Nature Communications*, *13*(1), 7396. https://doi.org/10.1038/s41467-022-34934-x

Zickfeld, K., Azevedo, D., Mathesius, S., & Matthews, H. D. (2021). Asymmetry in the climate–carbon cycle response to positive and negative CO2 emissions. *Nature Climate Change*, *11*(7), 613-617. https://doi.org/10.1038/s41558-021-01061-2